Broad-Spectrum Antimicrobial Supramolecular Assemblies with Distinctive Size and Shape

Kazuki Fukushima,[†,‡] Jeremy P. K. Tan,[§] Peter A. Korevaar,[⊥] Yi Yan Yang,[§,*] Jed Pitera,[†,*] Alshakim Nelson,[†] Hareem Maune,[†] Daniel J. Coady,[†] Jane E. Frommer,[†] Amanda C. Engler,[†] Yuan Huang,[∥] Kaijin Xu,[¶] Zhongkang Ji,[¶] Yuan Qiao,[§] Weimin Fan,[∥,#] Lanjuan Li,[¶] Nikken Wiradharma,[§] E. W. Meijer,[⊥] and James L. Hedrick[†,*]

[†]IBM Almaden Research Center, 650 Harry Road, San Jose, California 95120, United States, [‡]Department of Polymer Science and Engineering, Yamagata University, Yonezawa, Yamagata 992-8510, Japan, [§]Institute of Bioengineering and Nanotechnology, 31 Biopolis Way, The Nanos, Singapore 138669, Singapore, [⊥]Institute for Complex Molecular Systems, Eindhoven University of Technology, P.O. Box 513, 5600 MB Eindhoven, The Netherlands, [∥]Program of Innovative Therapeutics and [¶]State Key Laboratory for Diagnosis and Treatment of Infectious Diseases, The First Affiliated Hospital, College of Medicine, Zhejiang University, China, and [#]Department of Pathology and Laboratory Medicine, Medical University of South Carolina, Charleston, South Carolina 29425, United States

ABSTRACT With the increased prevalence of antibiotic-resistant infections, there is an urgent need for innovative antimicrobial treatments. One such area being actively explored is the use of self-assembling cationic polymers. This relatively new class of materials was inspired by biologically pervasive cationic host defense peptides. The antimicrobial action of both the synthetic polymers and naturally occurring peptides is believed to be complemented by their three-dimensional structure. In an effort to evaluate shape effects on antimicrobial materials, triblock polymers were polymerized from an assembly directing terephthalamide-bisurea core. Simple changes to this core, such as the addition of a methylene spacer, served to direct self-assembly into distinct morphologies—spheres and rods. Computational modeling also demonstrated how subtle core changes could directly alter urea stacking motifs manifesting in unique multidirectional hydrogen-bond networks despite the vast majority of material consisting of poly(lactide) (interior block) and cationic polycarbonates (exterior block). Upon testing the spherical and rod-like morphologies for antimicrobial properties, it was found that both possessed broad-spectrum activity (Gram-negative and Gram-positive bacteria as well as fungi) with minimal hemolysis, although only the rod-like assemblies were effective against *Candida albicans*.

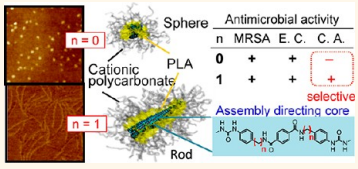

KEYWORDS: supramolecular assemblies · biodegradable polymers · antimicrobial · broad-spectrum activity · clinically isolated microbes · multidrug resistance

In the past decade, there has been an enormous increase in antibiotic-resistant bacteria, such as methicillin-resistant *Staphylococcus aureus* (MRSA), vancomycin-resistant *Enterococcus* (VRE) and fluoroquinolone-resistant *Escherichia coli*.[1] Most modern antibiotics act on specific molecular targets within bacteria. This yields therapeutic specificity but allows resistance development through mutation (among other mechanisms) since the bacterial cell morphology is generally preserved. In contrast, certain cationic host defense peptides act on the entire cellular membrane *via* electrostatic attraction and subsequent pore generation.[2] This ultimately leads to cell membrane destabilization and death. These naturally occurring compounds are typically found to have minimum inhibitory concentrations (MICs) ranging from 1 to >100 μg/mL, depending on both the properties of the peptides and the test conditions.[3−5] Polymeric synthetic analogues which have been attempted to mimic host defense peptide structure and function as well as reduce production cost include, but are not limited to, polynorbornene[6−9] and polyacrylate derivatives,[10−12] poly(arylamide),[13] poly(β-lactam),[14] polyethyleneimines,[15,16] and poly(α-amino acids) from *N*-carboxyanhydrides,[17,18] and pyridinium homopolymers and copolymers[19] have shown MIC values ranging from 4 to >1000 μg/mL.[6−19] In general, the overall hydrophobic/hydrophilic balance of polymers affects antimicrobial activity and selectivity toward bacteria.[20,21] Though a variety of amphiphilic polymers have been tested, few have shown activity against both Gram-negative and Gram-positive bacteria, especially while using a biodegradable/compatible platform.[17,18,22,23]

In the parallel research field of nanostructured materials for drug delivery, effects of nanoparticle size on cellular uptake and circulation time have been well-established, with particle sizes below 200 nm being considered optimal.[24] It is widely accepted

* Address correspondence to hedrick@almaden.ibm.com, pitera@us.ibm.com, yyyang@ibn.a-star.edu.sg.

Received for review August 4, 2012 and accepted September 21, 2012.

Published online September 21, 2012
10.1021/nn3035217

that both size and shape play critical roles in determining how particles navigate biological barriers.[25] For example, high aspect ratio single-walled carbon nanotubes have been shown to penetrate cells and transport a variety of cargos including peptides, genetic material, and drugs.[26,27] DeSimone and co-workers addressed these questions in a fundamental way using the "PRINT" nanofabrication technique to create polymeric nanoparticles of discrete, well-defined sizes and shapes.[28] However, systematic studies for determining analogous structure–activity effects on antimicrobial materials have received considerably less attention.

A particularly attractive way to achieve particles with precise shape, size, and dynamics is through directed self-assembly. High aspect ratio nanostructured materials have emerged from programmed assembly of molecules using noncovalent interactions such as hydrogen bonds, van der Waals forces, hydrophobic effects, $\pi-\pi^*$ stacking, ion–ion, ion–dipole, and dipole–dipole interactions.[29] Self-assembling moieties with complementary hydrogen-bonding groups in the core often result in columnar nanostructures[30] as well as triblock copolymers having urea groups in the central block.[31,32] Peptide-based amphiphiles forming micrometer long nanofibers stabilized by van der Waals forces and hydrogen bonding have exemplified self-assembling materials with biomedical applications.[33,34] The formation of high aspect ratio self-assemblies often involves a nucleation mechanism where energetically unfavorable fiber formation must precede favorable fiber elongation.[35] This mechanism favors growth of fewer long fibers instead of many short ones. Assembly shape materials can be further controlled by specifically tuning different noncovalent interactions. Balancing attractive noncovalent forces within the hydrophobic core using electrostatic repulsive interactions toward the hydrophilic periphery can facilitate switching from spherical to high aspect ratio assemblies.[36] Similarly, varying hydrophilic and hydrophobic branched segments of Janus dendrimers yields a wide variety of morphologies in water, including high aspect ratio tubular vesicles and helical ribbons.[37] Block copolymers, as a class of amphiphiles, offer considerable diversity in chemical and physical properties[38,39] including "Y-junctions" that assemble into a three-dimensional network of cylindrical micelles,[40] toroidal micelles,[41] one-dimensional chains of micelles,[42] multicompartment vesicles,[43] and complex cylindrical co-micelles *via* nucleation and growth processes.[44]

In order to bridge these two emerging fields—antimicrobial polymers and directed self-assembly—we designed a nanostructured system for comparing spherical and rod-shaped morphologies. Both shapes were found to have similar size and charge density, permitting a comparison of structural effects. In this study, we aimed to develop broad-spectrum antimicrobials and elucidate the role of size and shape in antimicrobial activity. Previously, we reported a simple approach that transformed spherical micelles into nanorods or nanotubes *via* incorporation of a benzamide-urea hydrogen-bonding unit at the block junction.[45] Analogous to that system, antimicrobial triblock polymers were designed to elongate rather than form spherical structures. This was accomplished using a rigid hydrophobic terephthalamide-bisurea core flanked by hydrophobic polylactide blocks (either L-, D-, or *rac*-PLA) along with periphery hydrophilic polycarbonate blocks having cationic propyl trimethylammonium bromides for antimicrobial properties. Two different bisurea cores were studied, one with and the other without a flexible methylene spacer between terephthalamide and aryl urea groups ($n = 0$ or 1 in Figure 1). The urea cores were modeled and shown to have considerably different bonding patterns giving rise to unique aggregation motifs. The spherical and rod-like micelles displayed broad-spectrum targeted activity against Gram-positive and Gram-negative bacteria as well as fungi without any significant toxicity toward mammalian cells (*i.e.*, red blood cells).

RESULTS AND DISCUSSION

A key design feature in the antimicrobial triblock polymers was the rigid terephthalamide-bisurea cores bearing dual inititiating moieties. The initiators permitted two facially opposed block polymers to be installed simultaneously creating a pseudo triblock polymer with centrally located hydrogen-bonding functionalities (Figure 1). The cores were constructed in a one-pot synthesis through reaction of diamine **1a**, or **1b**, with bis(pentafluorophenyl)carbonate (PFC) generating a reactive carbamate. Subsequent addition of 5-amino-1-pentanol formed the bis-urea core while concurrently installing two ROP initiating hydroxyl groups (**2a** and **2b**, respectively). Using the previously reported catalyst system of *N*-(3,5-bis(trifluoromethyl)-phenyl-*N*′-cyclohexylthiourea (TU) and 1,8-diazabicyclo[5.4.0]undec-7-ene (DBU), the ROP of lactide (L-, D-, or *rac*-) formed macroinitiators **2a** and **2b** used to synthesize polymer sets **3a** and **3b** (the lactide stereochemistry is denoted by the last character, *i.e.*, **3a-L**), respectively. It should also be noted that lactide polymerizations were conducted in DMSO due to the limited solubility of the urea initiators (**2a** and **2b**) in standard ROP solvents. The degree of polymerization (DP), relative M_n, polydispersity (PDI), and polylactide enantiomeric purity were determined using ^{1}H NMR, ^{13}C NMR, and gel permeation chromatography (GPC) for all polymers evaluated (Figure S1 in the Supporting Information). The outer carbonate blocks were polymerized from macroinitiator sets **3a** and **3b** in DCM, thus forming procationic polymer sets **4a** and **4b** using 2-(3-bromopropyl)oxycarbonyl-2-methyl trimethylenecarbonate (MTC-BP). Upon complete

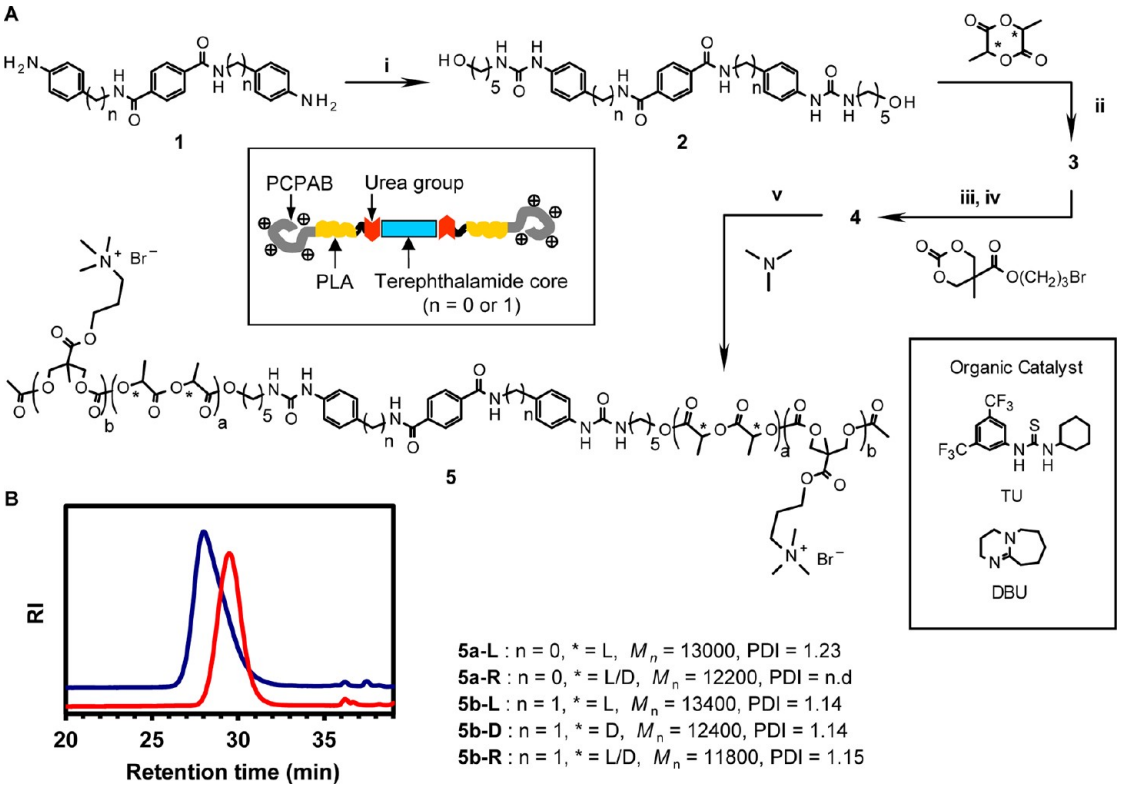

Figure 1. Synthesis of triblock copolymers 5. (*A*) Synthesis scheme, (i) $(C_6F_5O)_2CO$, 5-amino-1-pentanol, DMF; (ii) 5% TU catalyst, 5% DBU, DMSO; (iii) 2.5% TU catalyst, 2.5% DBU, methylene chloride; (iv) Ac_2O and (v) acetonitrile/DMF (1:1). (*B*) GPC chromatograms of 3b-L (red) and 4b-L (blue): measured at 30 °C in THF.

TABLE 1. Physicochemical and Biological Properties of Nanostructures

				MIC (mg/L)					
				Gram-positive			Gram-negative	fungus	yeast
polymer	diameter, nm (aspect ratio)	CMC[a] (mg/L)	ζ-potential[b] (mV)	S. aureus	MRSA	VRE	E. coli	C. neoformans	C. albicans
5a-L	20.4 (1)	35.5 (36.3)	19.1 ± 0.6 (21.2 ± 1.7)	150	75	30	75	20	>500
5b-L	10 (≥10)	25.1 (31.6)	15.2 ± 1.4 (25.1 ± 1.4)	75	40	75	100	20	75
5b-D	10 (≥10)	27.1 (28.2)	17.3 ± 0.7 (27.1 ± 1.8)	100	75	75	100	20	75
5b-R	10 (≥10)	50.1 (56.2)	21.7 ± 0.4 (29.7 ± 1.3)	75	75	50	100	20	100
5b-L + 5b-D	10 (≥10)	12.6 (15.8)	17.8 ± 0.9 (25.6 ± 1.0)	75	100	75	150	20	>150

[a] Measured in MH broth. The values in parentheses were measured in a simulated growth medium with salt concentration of 100 mM. [b] Polymer concentration: 1 mg/mL.

monomer conversion, excess acetic anhydride was added to quench the polymerization and acetylate the reactive chain ends followed by precipitation into MeOH. The quaternization reaction was conducted in DMF/CH_3CN (1/1) using trimethylamine (TMA) to form cationic triblock polymers **5a** and **5b** (Figure 1).

The copolymers formed supramolecular structures when dissolved in water above their respective critical micelle concentration (CMC)—between 13 and 50 mg/L measured in Mueller–Hinton broth (MHB) medium (Table 1 and Figure S2). The polymer solutions were effectively processed from water *via* spin-coating (AFM imaging) or direct-casting (TEM and cryo-TEM imaging). Morphological disparities between polymer sets **5a** and **5b** were considerable despite differing by only two carbons. Furthermore, polymer series **5a** produced spherical micelles (regardless of lactide stereochemistry) with an average diameter of 20.4 nm (PDI = 0.13) and an aggregation number of eight, while polymer series **5b** (irrespective of lactide stereochemistry) formed high aspect ratio filament-like structures with diameters just below 10 nm and lengths of up to or greater than 100 nm as estimated by AFM and TEM (Figure 2 and Figures S1 and S3). Mixtures of L- and D-lactide are known to form stereocomplexes with improved kinetic stability and lowered CMC values.[46] The mixtures of polymers **5b-L** and **5b-D** retained their high aspect ratio rod-like structure with

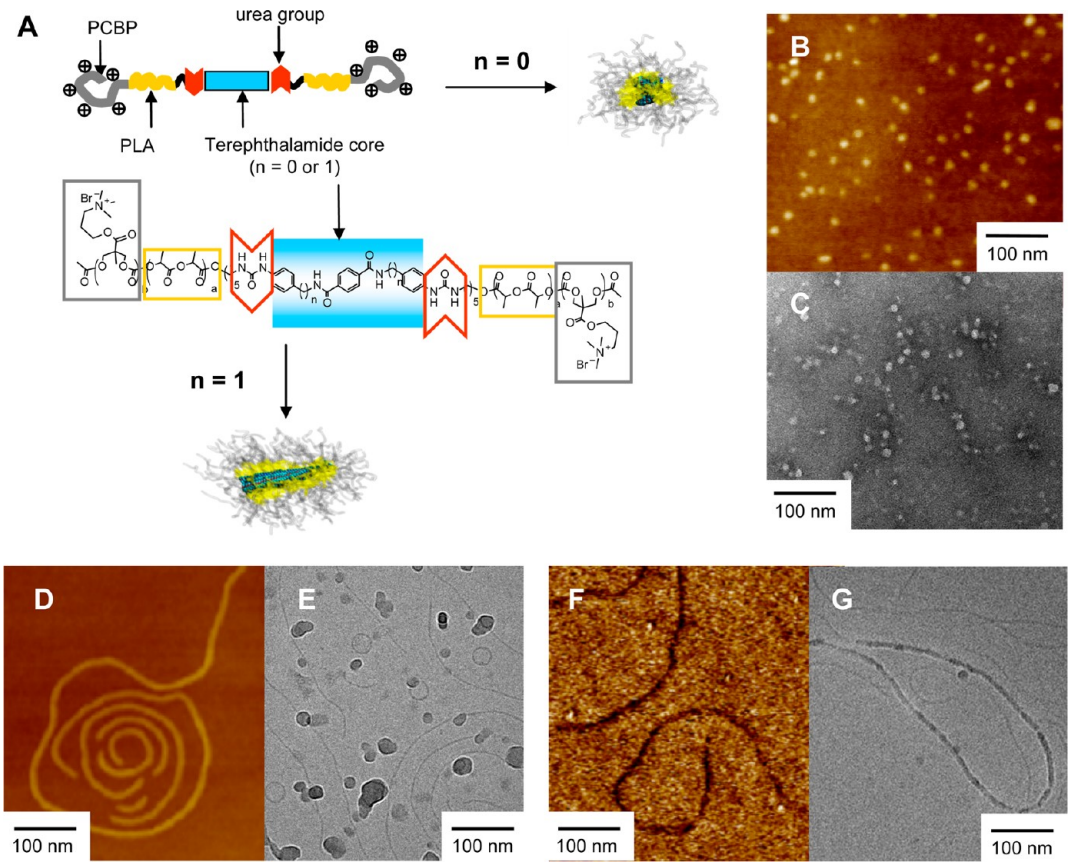

Figure 2. Self-assembly of triblock copolymers 5. Schematic representation (A), AFM images (B,D,F) and TEM images (C,E,G) of 5a-L (B,C), 5b-R (D,E), and 5b-L + 5b-D (F,G). Images E and G were obtained using cryo-TEM.

a slightly depressed CMC value (Table 1). These combined results showed that lactide stereochemistry played a minimal role in structural size and shape determinations. The data obtained from computational predictions, TEM, cyro-TEM, and AFM on assembly shape and size all proved to be consistent within experimental error, confirming the two distinct morphologies. It is also noteworthy that polymer assemblies were formed in pure water rather than media broth for ease of characterization. This was deemed acceptable because negligible differences were found between the water and broth medium when determining CMC (Table 1).

Computational models were employed to understand how the addition of methylene spacers radically changed supramolecular architecture. Using molecular mechanics conformational analysis on the terephthalamide-bisurea core revealed a preferred rigid rod-like geometry for **2a** and a zigzag or bent structure for **2b** (Figure 3A). Low-energy dimer structures (Figure 3B) were expanded into nanorod geometries (Figure 3C) and simulated with a hybrid molecular mechanics/coarse-grained model where lactide and carbonate polymers were represented using simplified coarse-grained potentials based on relative physical polymer models (Figure 3D,E). In the case of core **2b**, the molecules packed in a flat sheet where urea hydrogen bonds and $\pi-\pi^*$ stacking directed assembly. This planar structure was buttressed by additional layers that coupled to one another through amide hydrogen bonding. Simulations indicated that the reduced molecular freedom of **5a** permitted only a single-layer nanorod structure (a similar structure could also be modeled for polymer set **5b** but was determined to be inoperative due to rod formations) that was unstable at room temperature, causing collapse into a spherical geometry. Additionally, polymer set **5b** was able to form a two-layer nanorod structure of considerably greater stability due to flexibility granted by the methylene spacers. Modeling further demonstrated that the two-layer nanorod structures exhibited minimal structural fluctuations as confirmed by TEM and AFM analyses (Figure S4).

The cationic assemblies (spherical or rod-like) were evaluated for antimicrobial activity. Their overall net charges were determined in MHB *via* measuring respective ζ-potentials. All materials were found to have potentials ranging from 15 to 22 mV (Table 1), allowing efficient electrostatic interactions with the anionic microbial cell wall and cell membrane. Antimicrobial activities were investigated using clinically relevant and clinically isolated Gram-positive (*Staphylococcus aureus*), drug-resistant Gram-positive MRSA and VRE, and Gram-negative (*E. coli*) bacteria, as well as fungi (*Candida albicans* and *Cryptococcus neoformans*) (Figures S5–7).

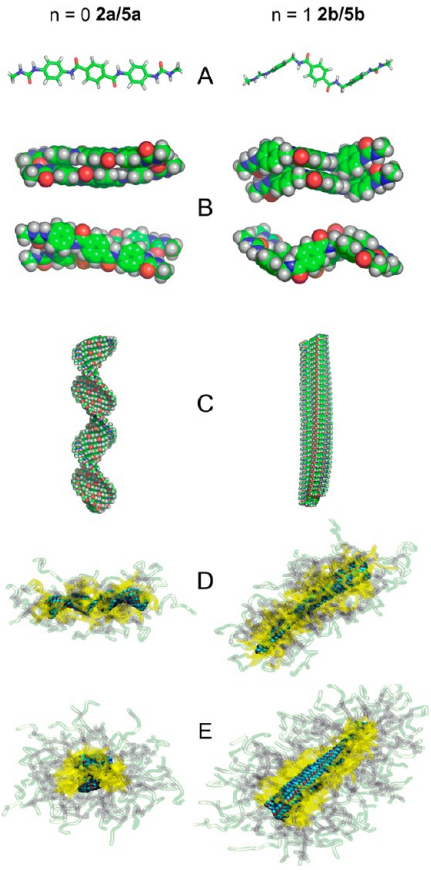

Figure 3. Molecular modeling of copolymer assembly. Images in the left column correspond to molecules without methylene spacers in the terephthalamide core (*n* = 0, 2a/5a); the right column corresponds to the methylene-containing core (*n* = 1, 2b/5b). (A) Stick representations of the minimum energy monomer conformation for each core. (B) Side and top views of the minimum energy dimer conformations for each core in a space-filling representation. (C) Supramolecular assemblies built from the minimum energy dimer structures, a helix for *n* = 0 and a multilayered sheet for *n* = 1. (D) Supramolecular assemblies with coarse-grained polylactide in transparent yellow and polycarbonate in transparent gray. After Langevin dynamics, the *n* = 0 helix collapses to a spherical micelle (E, left) while the *n* = 1 nanorod is stable (E, right).

As listed in Table 1, the cationic nanorods **5b-L**, **5b-D**, **5b-R**, and **5b-L** + **5b-D** effectively inhibited growth of all microbes with relatively low MIC values (except for the **5b-L** + **5b-D** stereocomplex against *Candida albicans*). Interestingly, the broad-spectrum activity of **5a** against both Gram-negative and Gram-positive bacteria was not found in our previous report,[22] which likely stems from smaller sized micelles (~20 nm) resulting from lowered aggregation number (~8). Moreover, it showed the powerful influence made by terephthalamide-bisurea cores on assembly and subsequent antimicrobial properties. Although **5a** had broad-spectrum activity, it failed to eradicate fungus growth up to polymer concentrations of 500 mg/L. Notably, both *Candida albicans*[47] and *Cryptococcus neoformans*[48] have significantly thicker cell walls (~280 and 190–210 nm, respectively) than Gram-positive bacteria (~20–80 nm).[49] Additionally, the cell wall of *Candida albicans* also consists of multiple layers[50] and is considerably less negatively charged than that of *Cryptococcus neoformans* (ζ-potential = −4 and ~−30 mV,[51] respectively). As a result, cationic nanoparticles have increased difficultly in adhering to the *Candida albicans* cell wall in order to act on membranes and cause disruption and lysis. Polymers **5b** had relatively stronger activities against *Candida albicans*. These results are considered important as a major challenge in developing antifungal drugs stems from the limited fungi-specific targets, as fungi are metabolically similar to mammalian cells. Nonetheless, the broad-spectrum activity of both **5a** and **5b** against Gram-negative and Gram-positive targets was somewhat unexpected given the dramatic differences in assembly morphology. As previously mentioned, the CMC values in both broth and water were nearly identical, suggesting that the morphology in broth was identical to that of water.

In order to determine microbicidal properties, colony assays were performed. Microbial samples treated with polymer set **5b** for 8 (*Staphylococcus aureus*, MRSA, VRE, and *E. coli*) or 18 h (*Candida albicans* and *Cryptococcus neoformans*) showed nearly 100% eradication using polymer concentrations around or less than two times above their MICs, indicating a microbicidal mechanism.

The antimicrobial mechanism was studied by visualizing the microbial cell structure (*i.e.*, MRSA, *E. coli*, and *C. albicans*) before and after polymer treatment using TEM imaging. Prior to treatment, all microbes showed intact structure (Figure 4, control). After treatment with **5b-R**, cell wall and membrane damage was easily visible along with dead microbe remnants (Figure 4, treated). Membrane disintegration was further investigated using FITC-labeled dextran dye (40 kDa) and confocal microscopy. After treating *S. aureus* and *E. coli* with **5b-R** at MICs (75 and 100 mg/L, respectively) and 200 mg/L (>MIC) for 30 min, uptake of labeled dextran by passive diffusion was measured. As shown in Figure 5, no FITC dextran uptake was seen for the untreated control cells, whereas cells exposed to **5b-R** at both concentrations led to significant uptake, indicating that the assemblies were acting by rupturing the bacterial membrane. In a similar experiment, membrane damage induced on fungi was evaluated *via* measuring the absorbance (260 nm) caused by nucleic acid release into the culture media.[46] After treatment of *C. albicans* with **5b-R**, the concentration of cytoplasmic constituents was found to exhibit a dose-dependent relationship (Figure S8), indicating that **5b-R** caused cell membrane damage. Additionally, most MICs listed in Table 1 were found to be greater than the CMCs, indicating that triblock polymers were acting as aggregate assemblies rather than discrete polymer chains.

A major side effect caused by many cationic antimicrobial peptides and polymers is hemolysis.[20]

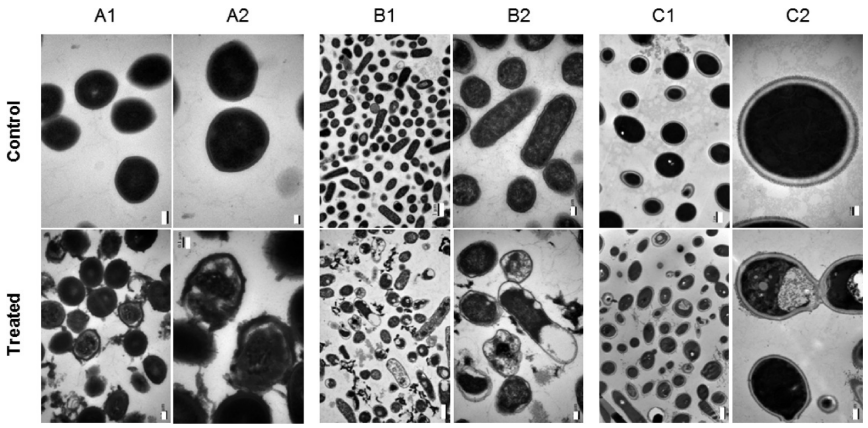

Figure 4. Antimicrobial activity of 5b-R copolymer assemblies. TEM images of methicillin-resistant S. aureus (A), E. coli (B), and C. albicans (C) before (control) and after incubation with 5b-R for 8 h at a lethal dose of 200 mg/L, which is slightly above the MICs. After the treatment, the cell wall and membrane were damaged, and cell death was observed. Moreover, in E. coli, precipitation of cytoplast was found. In C. albicans, large empty space in the cytosol and burst of cytoplast were also seen. Size of the bars: 0.2 μm for A1 (control and treated); 0.1 μm for A2 (control and treated); 1 μm for B1 (control and treated); 0.2 μm for B2 (control and treated); 1 and 2 μm for C1 (control and treated), respectively; 0.2 and 0.5 μm for C2 (control and treated), respectively.

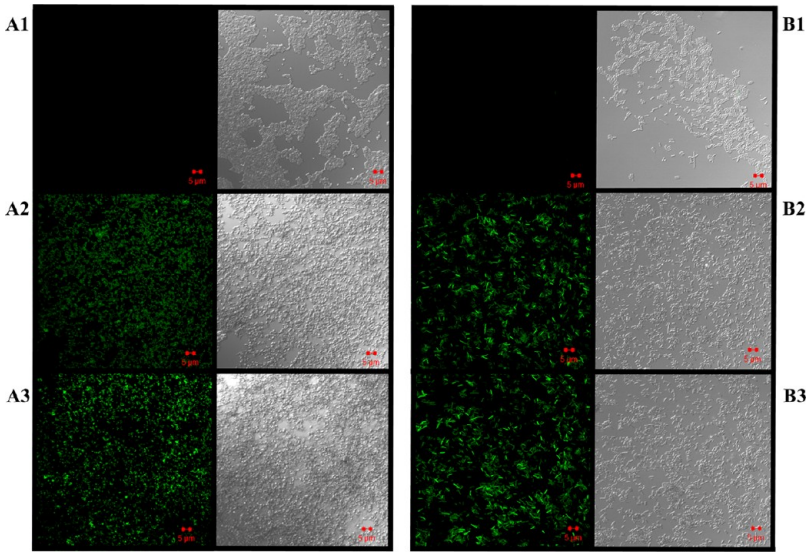

Figure 5. Confocal microscopic images of S. aureus (A) and E. coli (B) incubated with 5b-R for 30 min at concentrations of 0 (1), MICs (2), and 200 mg/L (3, slightly above the MICs) in the presence of FITC-conjugated dextran (40 kDa). Uptake of FITC-labeled dextran molecules was seen after the treatment with 5b-R at both concentrations, indicating membrane disruption. Scale bar: 5 μm.

Previous reports have highlighted criterion which greatly aid in increasing selectivity and were readily incorporated into both our spherical and rod systems.[9,10,19,20,52] Hemolytic evaluations were conducted using rat red blood cells incubated with polymers at various concentrations. Negligible hemolytic activity was observed for all polymers, even at concentrations well above what would be utilized therapeutically (1000−5000 μg/mL) (Figure S9), demonstrating their excellent selectivity.[53]

CONCLUSIONS

In this study, a new class of biodegradable cationic antimicrobial nanoparticles has been developed using a terephthalamide-bisurea core to initiate triblock polymers of lactide and cyclic carbonates using organocatalyzed ring-opening polymerization. The core, comprising both hydrogen-bond donors and acceptors, directed self-assembly into either spherical or rod-like three-dimensional cationic structures. Through computational modeling, it was found that differences in three-dimensional structures were directly attributable to small changes (2 carbons) in the terephthalamide-bisurea core. These subtle changes altered the hydrogen-bonding stacking motif, significantly affecting larger morphological features. Both types of spherical and rod-shaped assemblies exhibited broad-spectrum antimicrobial activity and minimal

mammalian cell toxicity (*i.e.*, hemolysis). Therefore, these nanostructures are promising antimicrobial agents. In addition, the design principle of these nanostructures provides guidance for making functional high aspect ratio nanostructures for many other applications.

METHODS

Morphology Observation of Block Copolymers. AFM samples were prepared *via* dialysis of the polymer (20 mg in 2 mL DMF + 4 mL water) against deionized water (1 L) using a Spectra/Por dialysis bag (MWCO = 1000 g/mol). The sample was dialyzed for 2 days, changing the water at least three times. After dialysis, the polymer solution was diluted with water (2 mL) and spin-coated on a silicon wafer (1 in.) at 3000 rpm for 30 s. After drying overnight in vacuum, the samples were used for AFM studies without further processing. The morphologies of micelles formed from block copolymers were characterized with atomic force microscopy (AFM) using a Digital Instruments Dimension 3100 in tapping mode, bearing a standard silicon cantilever.

The morphologies of the micelles were also observed under a FEI Tecnai G^2 F20 electron microscope using an acceleration voltage of 200 keV. Five microliters of polymeric solution was left on the Formvar/carbon-coated 200 mesh copper grid for 1 min before the excess was removed by filter paper. Next, 5 μL of 0.2% (w/v) phosphotungtic acid (PTA) was pipetted onto the same copper grid and left for a minute. After that, the excess solution was again dried with filter paper before leaving to dry under an ambient condition. Additional TEM experiments using cryo-TEM were performed on the samples without a staining procedure and kindly supported by FEI company's application laboratory in Tsinghua University, China.

Minimal Inhibitory Concentration (MIC) Determination. *Staphylococcus aureus* and *E. coli* were obtained from ATCC and grown in MHB at 37 °C. Methicillin-resistant *Staphylococcus aureus*, vancomycin-resistant *Enterococcus*, and *Candida albicans* and *Cryptococcus neoformans* were extracted from patients' blood (methicillin-resistant *Staphylococcus aureus* and vancomycin-resistant *Enterococcus*), phlegm (*C. albicans*), and cerebrospinal fluid (*Cryptococcus neoformans*) samples, kindly provided by Z. Q. Wei, Department of Infectious Diseases, The First Affiliated Hospital, College of Medicine, Zhejiang University, P.R. China. The clinical samples were also grown in MHB at 37 °C. The MICs of the polymers were measured using a broth microdilution method. Briefly, 50 μL of polymer solution in water with various concentrations was placed into each well of 96-well plates. Fifty microliters of microorganism solution at a concentration that gave an optical density reading of ~0.1 at 600 nm was added to each well. The optical density readings of microorganism solutions were measured as a function of time. The MIC was taken at the concentration at which no growth was observed with the unaided eyes and microplate reader (Bio-Teck Instruments, Inc.) and in the growing phase of the microorganisms. Broth containing cells alone was used as the control. The tests were repeated at least three times.

Transmittance Electron Microscopy (TEM). The morphologies of the microorganisms before and after treatment with the nanostructures were observed under a JEM-1230 transmittance electron microscope (JEOL, Japan) using an acceleration voltage of 80 keV. The microorganism solution (1.5 mL) was incubated with 0.5 mL of micelle solution (200 mg/L) for 8 h. The solution was centrifuged at 5000 rpm for 10 min, and the supernatant was removed. Phosphate buffer (pH7.0, 0.5 mL) containing 2.5% glutaraldehyde was added to the microorganisms and incubated overnight at 4 °C for fixation. The sample was washed three times with the phosphate buffer (15 min each) and then postfixed with 1% OsO_4 in the phosphate buffer (pH7.0) for 1 h. The fixed sample was washed three times in the phosphate buffer (15 min each), followed by dehydration in a graded ethanol series.

The sample was incubated with the mixture of acetone and Spurr resin (1:1 in volume) for 1 h at room temperature, which was then transferred to 1:3 mixture of acetone and Spurr resin for 3 h, and to Spurr resin for overnight. Ultrathin sections (70−90 nm) were cut using a Reichert-Jung Ultracut E ultramicrotome and poststained with uranyl acetate and lead citrate for 15 min each prior to TEM observations.

Microbial Membrane Integrity Test. Two experiments were devised to test the microbial membrane integrity. If the integrity of the microbial membrane was compensated by its interaction with the nanostructures through pore formation, macromolecules could penetrate across such porous membranes. In our previous work, FITC-labeled dextran was used as an extracellular probe to characterize the presence of such pores in bacterial membrane treated with membrane-lytic peptides.[54] Similarly, the leakage of cytoplasmic constituents such as nucleic acids with absorbance at 260 nm (*i.e.*, 260 nm absorbing materials) was proposed to detect the integrity of the microbial membrane upon treatment with membrane-lytic agents.[55] These two methods were used in this study in order to show that the treatment of bacteria and/or fungi with **5b-R** nanostructures results in loss of microbial membrane's integrity. For these tests, microbial cells were inoculated overnight and diluted to give an o.d. reading of 0.1 before use.

To detect if probe macromolecules can passively diffuse into bacterial cells after the treatment with the nanostructures, confocal experiments were performed. Roughly, 500 μL of microbial suspension was treated simultaneously with 250 μL of FITC-labeled dextran (M_w = 40 kDa) and 250 μL of **5b-R** solution (or deionized water as negative control). The final concentration of each component in the suspension is ~3 × 10^8 CFU/mL for bacteria, 500 mg/L for FITC dextran, and corresponding MIC concentrations or 200 mg/L for **5b-R**. Under this condition, the bacterial suspension was incubated at 37 °C for 30 min, followed by centrifuging (3000*g*, 5 min) and phosphate-buffered saline (PBS) washing for two cycles. The cells were then fixed with 2.5% glutaraldehyde, washed two times with PBS, and resuspended. The cell suspension was spotted onto a poly-L-lysine-coated glass slide and incubated at room temperature for several hours. After that, the non-adhering cells were washed away with PBS and the cells were imaged under a confocal microscope.

To elucidate that the membrane damage after the treatment caused leakage of intracellular contents, the presence of 260 nm absorbing molecules in the culture media was tested after 3 h of incubation with the nanostructures. Roughly, 500 μL of microbial suspension was treated with 500 μL of **5b-R** solution at a concentration of 100 or 200 mg/L, which corresponds to MIC or 2 × MIC concentration for *C. albicans*. The suspension was shaken at room temperature at 250 rpm for 3 h and then filtered with a 0.22 μm filter to remove the microbial cells. Absorbance of the supernatant was measured at 260 nm in triplicate, and its value was normalized to the absorbance of untreated *C. albicans* solution.

Conflict of Interest: The authors declare no competing financial interest.

Acknowledgment. This work was funded by IBM Almaden Research Center (USA), Institute of Bioengineering and Nanotechnology (Singapore), Eindhoven University of Technology (The Netherlands), Zhejiang University (China), and Medical University of South Carolina (USA).

Supporting Information Available: Additional experimental procedures and figures. This material is available free of charge *via* the Internet at http://pubs.acs.org.

REFERENCES AND NOTES

1. Taubes, G. The Bacteria Fight Back. *Science* **2008**, *321*, 356–361.

2. Chan, D. I.; Prenner, E. J.; Vogel, H. J. Tryptophan- and Arginine-Rich Antimicrobial Peptides: Structures and Mechanisms of Action. *Biochim. Biophys. Acta, Biomembr.* **2006**, *1758*, 1184–1202.
3. Zasloff, M.; Martin, B.; Chen, H. C. Antimicrobial Activity of Synthetic Magainin Peptides and Several Analogues. *Proc. Natl. Acad. Sci. U.S.A.* **1988**, *85*, 910–913.
4. Blondelle, S. E.; Houghten, R. A. Hemolytic and Antimicrobial Activities of the Twenty-Four Individual Omission Analogs of Melittin. *Biochemistry* **1991**, *30*, 4671–4678.
5. Lee, K. H. Development of Short Antimicrobial Peptides Derived from Host Defense Peptides or by Combinatorial Libraries. *Curr. Pharm. Des.* **2002**, *8*, 795–813.
6. Al-Badri, Z. M.; Som, A.; Lyon, S.; Nelson, C. F.; Nusslein, K.; Tew, G. N. Investigating the Effect of Increasing Charge Density on the Hemolytic Activity of Synthetic Antimicrobial Polymers. *Biomacromolecules* **2008**, *9*, 2805–2810.
7. Ilker, M. F.; Nüsslein, K.; Tew, G. N.; Coughlin, E. B. Tuning the Hemolytic and Antibacterial Activities of Amphiphilic Polynorbornene Derivatives. *J. Am. Chem. Soc.* **2004**, *126*, 15870–15875.
8. Lienkamp, K.; Madkour, A. E.; Musante, A.; Nelson, C. F.; Nsslein, K.; Tew, G. N. Antimicrobial Polymers Prepared by ROMP with Unprecedented Selectivity: A Molecular Construction Kit Approach. *J. Am. Chem. Soc.* **2008**, *130*, 9836–9843.
9. Gabriel, G. J.; Maegerlein, J. A.; Nelson, C. F.; Dabkowski, J. M.; Eren, T.; Nsslein, K.; Tew, G. N. Comparison of Facially Amphiphilic *versus* Segregated Monomers in the Design of Antibacterial Copolymers. *Chem.—Eur. J.* **2009**, *15*, 433–439.
10. Ivanov, I.; Vemparala, S.; Pophristic, V.; Kuroda, K.; DeGrado, W. F.; McCammon, J. A.; Klein, M. L. Characterization of Nonbiological Antimicrobial Polymers in Aqueous Solution and at Water−Lipid Interfaces from All-Atom Molecular Dynamics. *J. Am. Chem. Soc.* **2006**, *128*, 1778–1779.
11. Kuroda, K.; DeGrado, W. F. Amphiphilic Polymethacrylate Derivatives as Antimicrobial Agents. *J. Am. Chem. Soc.* **2005**, *127*, 4128–4129.
12. Kenawy, E.-R.; Worley, S. D.; Broughton, R. The Chemistry and Applications of Antimicrobial Polymers: A State-of-the-Art Review. *Biomacromolecules* **2007**, *8*, 1359–1384.
13. Tew, G. N.; Liu, D. H.; Chen, B.; Doerksen, R. J.; Kaplan, J.; Carroll, P. J.; Klein, M. L.; DeGrado, W. F. *De Novo* Design of Biomimetic Antimicrobial Polymers. *Proc. Natl. Acad. Sci. U.S.A.* **2002**, *99*, 5110–5114.
14. Mowery, B. P.; Lee, S. E.; Kissounko, D. A.; Epand, R. F.; Epand, R. M.; Weisblum, B.; Stahl, S. S.; Gellman, S. H. Mimicry of Antimicrobial Host-Defense Peptides by Random Copolymers. *J. Am. Chem. Soc.* **2007**, *129*, 15474–15476.
15. Lin, J.; Qiu, S. Y.; Lewis, K.; Klibanov, A. M. Bactericidal Properties of Flat Surfaces and Nanoparticles Derivatized with Alkylated Polyethylenimines. *Biotechnol. Prog.* **2002**, *18*, 1082–1086.
16. Mukherjee, K.; Rivera, J. J.; Klibanov, A. M. Practical Aspects of Hydrophobic Polycationic Bactericidal "Paints". *Appl. Biochem. Biotechnol.* **2008**, *151*, 61–70.
17. Zhou, C. C.; Qi, X.; Li, P.; Chen, W. N.; Mouad, L.; Chang, M. W.; Leong, S. S. J.; Chan-Park, M. B. High Potency and Broad-Spectrum Antimicrobial Peptides Synthesized *via* Ring-Opening Polymerization of α-Aminoacid-*N*-carboxyanhydrides. *Biomacromolecules* **2010**, *11*, 60–67.
18. Engler, A. C.; Shukla, A.; Puranam, S.; Buss, H. G.; Jreige, N.; Hammond, P. T. Effects of Side Group Functionality and Molecular Weight on the Activity of Synthetic Antimicrobial Polypeptides. *Biomacromolecules* **2011**, *12*, 1666–1674.
19. Sambhy, V.; Peterson, B. R.; Sen, A. Antibacterial and Hemolytic Activities of Pyridinium Polymers as a Function of the Spatial Relationship between the Positive Charge and the Pendant Alkyl Tail. *Angew. Chem., Int. Ed.* **2008**, *47*, 1250–1254.
20. Palermo, E.; Kuroda, K. Structural Determinants of Antimicrobial Activity in Polymers Which Mimic Host Defense Peptides. *Appl. Microbiol. Biotechnol.* **2010**, *87*, 1605–1615.
21. Timofeeva, L.; Kleshcheva, N. Antimicrobial Polymers: Mechanism of Action, Factors of Activity, and Applications. *Appl. Microbiol. Biotechnol.* **2011**, *89*, 475–492.
22. Nederberg, F.; Zhang, Y.; Tan, J. P. K.; Xu, K.; Wang, H.; Yang, C.; Gao, S.; Guo, X. D.; Fukushima, K.; Li, L.; *et al.* Biodegradable Nanostructures with Selective Lysis of Microbial Membranes. *Nat. Chem.* **2011**, *3*, 409–414.
23. Salick, D. A.; Kretsinger, J. K.; Pochan, D. J.; Schneider, J. P. Inherent Antibacterial Activity of a Peptide-Based β-Hairpin Hydrogel. *J. Am. Chem. Soc.* **2007**, *129*, 14793–14799.
24. Alexis, F.; Pridgen, E.; Molnar, L. K.; Farokhzad, O. C. Factors Affecting the Clearance and Biodistribution of Polymeric Nanoparticles. *Mol. Pharmaceutics* **2008**, *5*, 505–515.
25. Geng, Y.; Dalhaimer, P.; Cai, S.; Tsai, R.; Tewari, M.; Minko, T.; Discher, D. E. Shape Effects of Filaments *versus* Spherical Particles in Flow and Drug Delivery. *Nat. Nanotechnol.* **2007**, *2*, 249–255.
26. Liu, Z.; Sun, X.; Nakayama-Ratchford, N.; Dai, H. Supramolecular Chemistry on Water-Soluble Carbon Nanotubes for Drug Loading and Delivery. *ACS Nano* **2007**, *1*, 50–56.
27. Prato, M.; Kostarelos, K.; Bianco, A. Functionalized Carbon Nanotubes in Drug Design and Discovery. *Acc. Chem. Res.* **2007**, *41*, 60–68.
28. Gratton, S. E. A.; Ropp, P. A.; Pohlhaus, P. D.; Luft, J. C.; Madden, V. J.; Napier, M. E.; DeSimone, J. M. The Effect of Particle Design on Cellular Internalization Pathways. *Proc. Natl. Acad. Sci. U.S.A.* **2008**, *105*, 11613–11618.
29. Anslyn, E. V.; Dougherty, D. A. *Modern Physical Organic Chemistry*, 1st ed.; University Science Books: Sausalito, CA, 2006.
30. Smulders, M. M. J.; Schenning, A. P. H. J.; Meijer, E. W. Insight into the Mechanisms of Cooperative Self-Assembly: The "Sergeants-and-Soldiers" Principle of Chiral and Achiral C3-Symmetrical Discotic Triamides. *J. Am. Chem. Soc.* **2007**, *130*, 606–611.
31. Chebotareva, N.; Bomans, P. H. H.; Frederik, P. M.; Sommerdijk, N. A. J. M.; Sijbesma, R. P. Morphological Control and Molecular Recognition by Bis-urea Hydrogen Bonding in Micelles of Amphiphilic Tri-block Copolymers. *Chem. Commun.* **2005**, 4967–4969.
32. Obert, E.; Bellot, M.; Bouteiller, L.; Andrioletti, F.; Lehen-Ferrenbach, C.; Boué, F. Both Water- and Organo-Soluble Supramolecular Polymer Stabilized by Hydrogen-Bonding and Hydrophobic Interactions. *J. Am. Chem. Soc.* **2007**, *129*, 15601–15605.
33. Hartgerink, J. D.; Beniash, E.; Stupp, S. I. Self-Assembly and Mineralization of Peptide-Amphiphile Nanofibers. *Science* **2001**, *294*, 1684–1688.
34. Haines-Butterick, L.; Rajagopal, K.; Branco, M.; Salick, D; Rughani, R.; Pilarz, M.; Lamm, M. S.; Pochan, D. J.; Schneide, J. P. Controlling Hydrogelation Kinetics by Peptide Design for Three-Dimensional Encapsulation and Injectable Delivery of Cells. *Proc. Natl. Acad. Sci. U.S.A.* **2007**, *104*, 7791–7796.
35. De Greef, T. F. A.; Smulders, M. M. J.; Wolffs, M.; Schenning, A. P. H. J.; Sijbesma, R. P.; Meijer, E. W. Supramolecular Polymerization. *Chem. Rev.* **2009**, *109*, 5687–5754.
36. Besenius, P.; Portale, G.; Bomans, P. H. H.; Janssen, H. M.; Palmans, A. R. A.; Meijer, E. W. Controlling the Growth and Shape of Chiral Supramolecular Polymers in Water. *Proc. Natl. Acad. Sci. U.S.A.* **2010**, *107*, 17888–17893.
37. Percec, V.; Wilson, D. A.; Leowanawat, P.; Wilson, C. J.; Hughes, A. D.; Kaucher, M. S.; Hammer, D. A.; Levine, D. H.; Kim, A. J.; Bates, F. S.; *et al.* Self-Assembly of Janus Dendrimers into Uniform Dendrimersomes and Other Complex Architectures. *Science* **2010**, *328*, 1009–1014.
38. Discher, D. E.; Eisenberg, A. Polymer Vesicles. *Science* **2002**, *297*, 967–973.
39. Basko, M.; Bednarek, M.; Billiet, L.; Kubisa, P.; Goethals, E.; Du Prez, F. Combining Cationic Ring-Opening Polymerization and Click Chemistry for the Design of Functionalized Polyurethanes. *J. Polym. Sci., Part A* **2011**, *49*, 1597–1604.
40. Jain, S.; Bates, F. S. On the Origins of Morphological Complexity in Block Copolymer Surfactants. *Science* **2003**, *300*, 460–464.

41. Cui, H.; Chen, Z.; Zhong, S.; Wooley, K. L.; Pochan, D. J. Block Copolymer Assembly *via* Kinetic Control. *Science* **2007**, *317*, 647–650.
42. Pochan, D. J.; Chen, Z.; Cui, H.; Hales, K.; Qi, K.; Wooley, K. L. Toroidal Triblock Copolymer Assemblies. *Science* **2004**, *306*, 94–97.
43. Li, Z.; Kesselman, E.; Talmon, Y.; Hillmyer, M. A.; Lodge, T. P. Multicompartment Micelles from ABC Miktoarm Stars in Water. *Science* **2004**, *306*, 98–101.
44. Wang, X. S; Guerin, G.; Wang, H.; Wang, Y. S.; Manners, I.; Winnik, M. A. Cylindrical Block Copolymer Micelles and Co-micelles of Controlled Length and Architecture. *Science* **2007**, *317*, 644–647.
45. Kim, S. H.; Nederberg, F.; Jakobs, R.; Tan, J. P. K.; Fukushima, K.; Nelson, A.; Meijer, E. W.; Yang, Y. Y.; Hedrick, J. L. A Supramolecularly Assisted Transformation of Block-Copolymer Micelles into Nanotubes. *Angew. Chem., Int. Ed.* **2009**, *48*, 4508–4512.
46. Nederberg, F.; Appel, E.; Tan, J. P. K.; Kim, S. H.; Fukushima, K.; Sly, J.; Miller, R. D.; Yang, Y. Y.; Waymouth, R. M.; Hedrick, J. L. Simple Approach to Stabilized Micelles Employing Miktoarm Terpolymers and Stereocomplexes with Application in Paclitaxel Delivery. *Biomacromolecules* **2009**, *10*, 1460–1468.
47. Klis, F. M.; Groot, P. D.; Hellingwerf, K. Molecular Organization of the Cell Wall of *Candida albicans*. *Med. Mycol.* **2001**, *39*, 1–8.
48. Cassone, A.; Simonetti, N.; Strippoli, V. Wall Structure and Bud Formation in *Cryptococcus neoformans*. *Arch. Microbiol.* **1974**, *95*, 205–212.
49. Salton, M. R. J.; Kim, K.-S. *Medical Microbiology*; University of Texas Medical Branch at Galveston: Galveston, TX, 1996.
50. Ruiz-Herrera, J.; Victoria Elorza, M.; Valentín, E.; Sentandreu, R. Molecular Organization of the Cell Wall of *Candida albicans* and Its Relation to Pathogenicity. *FEMS Yeast Res.* **2006**, *6*, 14–29.
51. Nosanchuk, J.; Casadevall, A. Cellular Charge of *Cryptococcus neoformans*: Contributions from the Capsular Polysaccharide, Melanin, and Monoclonal Antibody Binding. *Infect. Immun.* **1997**, *65*, 1836–1841.
52. Oda, Y.; Kanaoka, S.; Sato, T.; Aoshima, S.; Kuroda, K. Block *versus* Random Amphiphilic Copolymers as Antibacterial Agents. *Biomacromolecules* **2011**, *12*, 3581–3591.
53. Som, A.; Tew, G. N. Influence of Lipid Composition on Membrane Activity of Antimicrobial Phenylene Ethynylene Oligomers. *J. Phys. Chem. B* **2008**, *112*, 3495–3502.
54. Wiradharma, N.; Khan, M.; Yong, L.-K.; Hauser, C. A. E.; Seow, S. V.; Zhang, S.; Yang, Y.-Y. The Effect of Thiol Functional Group Incorporation into Cationic Helical Peptides on Antimicrobial Activities and Spectra. *Biomaterials* **2011**, *32*, 9100–9108.
55. Chen, C. Z.; Cooper, S. L. Interactions between Dendrimer Biocides and Bacterial Membranes. *Biomaterials* **2002**, *23*, 3359–3368.